Transport-reaction dynamics of particulateorganic matter and oxygen in riverbed sediments

Eric E Roden[1], Ecenur Bulur[2],Stephanie Ann Napieralski[2], Steven P Loheide III[2], Matthew Ginder-Vogel[2], Christopher Zahasky[1], Evan Arntzen[3], Ruby Ghosh[4]

[1]Department of Geoscience, University of Wisconsin-Madison, Madison, WI; [2]Department of Civil and Environmental Engineering, University of Wisconsin-Madison, Madison, WI; [3]Pacific Northwest NationalLaboratory, Richland, WA; [4]Opti O_2, LLC, Okemos, MI

BACKGROUND & PURPOSE

Introduction

The interface between rivers and alluvial sediments adjacent to them is a critical zone for ecological and biogeochemical processes (Boano et al., 2014). Large-scale changes in river stage can lead to extended flooding of the nearshore hyporheic zone, with major attendant impacts on hyporheic exchange flows (HEFs) (Zachara et al., 2020). Excursions in HEFs have important implications for the input and transformation of river-derived organic materials and nutrients in river corridors.

Fig.1. Columbia River basis, showing location of the Hanford Reach immediately downstream of the Priest Rapids Dam (inset). Source: US Army Corp of Engineers.

This study deals with the riverbed of the Columbia River (CR) in eastern Washington State (Fig.1). We are working in the vicinity of the Hanford 300 Area within the Hanford Reach (HR) of the CR (Fig.2). This and other locations within the HR experience large fluctuations in river stage (see Fig. 12), which take place both naturally on a seasonal basis, and on shorter time scales (hours to day) in conjunction with hydroelectric power dam operations (Zachara et al., 2016; Stegen et al., 2016).

Observational and modelling studies in the HR of the CR have demonstrated that the alluvium layer (i.e. the riverbed) exerts significant control on river corridor HEFs (Zachara et al., 2020), and is associated with elevated levels of biogeochemical activity (Moser et al., 2003; Stegen et al., 2016; Hou et al., 2017; Liu et al., 2017).

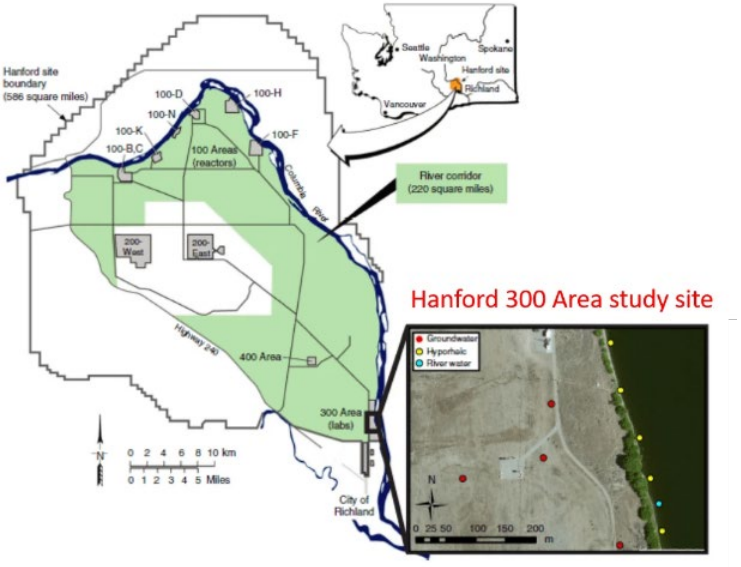

Fig. 2. Hanford Reach of the Columbia River illustrating Hanford 300 Area study site. Source: PNNL SFA.

Although accumulation of fine-grained particulate materials has long been recognized as a significant process in permeable

riverbed sediments (Brunke, 1999), the input and processing of particulate organic matter (POM) in riverbed sediments has been understudied (Trimmer et al., 2012) and remains an important knowledge gap (Graham et al., 2018; Yang et al., 2018). Large fluctuations in river stage create conditions conducive to the influx and transport of fine-grained POM (a biological colloid originating from the river water and/or in situ periphyton production), within near-surface riverbed sediments (Fig. 3).

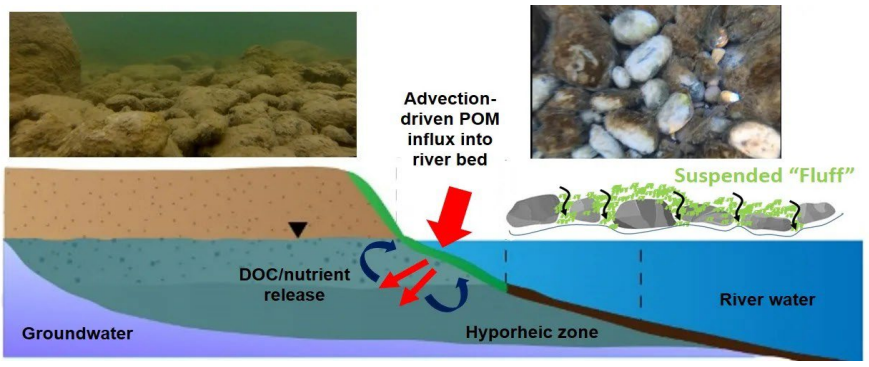

Fig. 3. Conceptual model for hydrologically (river stage) driven advective input of POM (suspended "fluff") into the riverbed at the Hanford 300 Area, leading to its accumulation in a near-surface sediment that underlies the armoring layer of large cobbles (see photos). River cross section diagram and upper left photo sources: PNNL SFA.

Purpose of Study

Much is known about dissolved organic matter (DOM) transport and metabolism in hyporheic zone sediments, but there is a paucity of quantitative information on POM dynamics and its influence on hyporheic zone biogeochemistry (e.g. dissolved oxygen dynamics). POM input has the potential to strongly impact the biogeochemistry of both the river itself as well as the hyporheic zone (Trimmer et al., Sci. Tot. Environ., 2012), with important implications for CO_2 and/or CH_4 production as well as retention and/or release of nutrients (e.g., N, P, S) associated with POM decomposition.

Recent studies have suggested that deposition of fresh POM can lead to elev ated rates of aerobic microbial metabolism, increased activity of anaerobic heterotrophic organisms, and release of labile dissolved organic carbon (DOC) in riverbed sediments from the Hanford 300 Area (Stern et al., 2017).

The central purpose of this study was to develop a hydrobiogeochemical model capable of simulating the transport and metabolism of POM and its impact on dissolved oxygen (DO) distribution within the riverbed as influenced by periodic changes in river stage and fluid flow rate and direction. The model was employed as a tool to interpret the results of *in situ* measurements of POM intrusion into the riverbed made using "POM traps" emplaced within the upper 20 cm of the riverbed, as well as *in situ* dissolved oxygen concentrations determined with a novel optical sensor buried directly in the riverbed at 20 cm depth.

EXPERIMENTAL METHODS & RESULTS

POM Trap Experiments

We developed a novel technique for estimating the input of fresh POM to near-surface Hanford 300 Area riverbed sediments (see Fig. 4 and embedded YouTube video), based on a prior approach used to quantify input of fine-grained materials to salmon bed environments within the HR of the CR (Hanrahan et al., 2007).

Fig. 4. Photo of POM trap deployed in the Hanford 300 Area riverbed, February 2020. See the following URL for a video of trap deployment and collection: (https://www.youtube.com/watch?v=jeWB6zTm2o8&fs=1&modestbranding=1&rel=0&showinfo=0)

Ashed bulk riverbed sediment (ca. 2 kg) is placed in baskets within collars embedded in the riverbed. The baskets are slotted to allow fluid and fine particle (< 100 uM) throughput. Traps were deployed for ca. 4-6 weeks in February/March and June/July 2020. Recovered materials were sieved to collect the < 0.25 mm fraction for POC/PON analysis. Separate POM addition experiments verified that this approach recovers virtually all added POM.

The results of the two deployment showed that the dry weight POC content in the < 0.25 mm fraction increased from a background of ca. 0.06% to up to 0.3%, corresponding to mmol/dm3 quantities of bulk POC accumulation (Fig. 5).

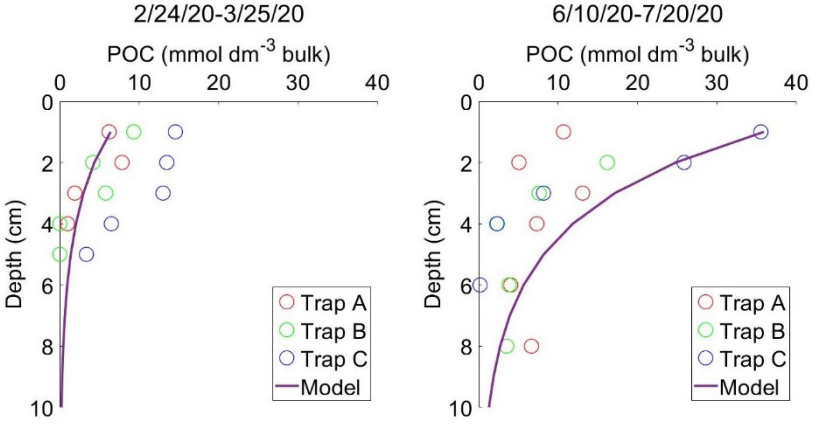

Fig. 5. Results of POM trap deployments in Feb-Mar and Jun-Jul 2020. Open symbols show measured POC accumulation; solid lines show results of transport-reaction model simulations for the time period of POM trap deployment.

POM Transport Experiments

The framework for modeling POM transport in riverbed sediments was adapted from the results of column transport experiments (Bulur, 2020; Bulur et al., 2021a,b) conducted with Hanford formation sediments and freshly-grown periphyton biomass from the Hanford 300 Area (Fig. 6). The experiments showed that the transport of POM could be described by a model (adapted from Harter et al., 2000) that includes reversible sorption and irrev ersible filtration.

In situ DO Probe Measurements

In collaboration with PNNL SFA personnel, Ghosh and colleagues at Opti O_2, LLC deployed novel in situ optical (molybdenum chloride cluster phosphorescence based) DO probes (Ghosh et al., 2011; 2019a,b, and Gooseff et al., 2019) at 20 ca. cm depth atthree locations at the Hanford 300 Area between August and December 2020. The results of one of the probe deployments (approximate location shown in Fig. 3) are shown in Fig. 7. Large periodic fluctuations in DO concentration were observed from Aug-Nov when temperatures were maximal and when (according to the transport- modeling results; see Fig. 14) and active fresh POM degradation was likely taking place.

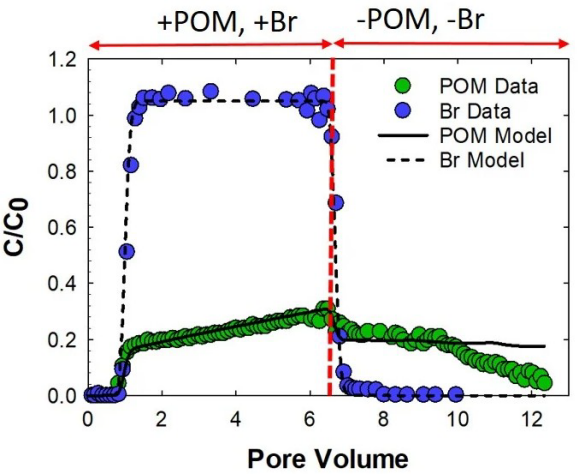

Figure 6. POM transport experiment with freshly-grown periphyton biomass (POM, ca. 1 mmol C/L) in columns (15 cm length x 2.5 cm diameter) packed with Hanford formation sediment (0.25-2 mm diameter). The solid line shows the results of a transport-reaction simulation that included reverible sorption/desorption and irreversible filtration of POM by the sediment matrix.

A k-means clustering analysis was conducted on the first derivatives of DO, specific conductivity, and water level (measured by a separate pressure sensor co-deployed at the same depth as the DO probe) with respect to time. Theresults revealed that temporal variations in DO during early August to early September were directly linked with variations in fluid conductivity (groundwater = high, river water = low). The variation in conductivity in turn reflected changes in fluid flux rate and direction driven by changes in water level. These results suggest a stronghydrological coupling between fluid advection rate/direction and DO, which was explored by transport-reaction modeling (see Fig. 15).

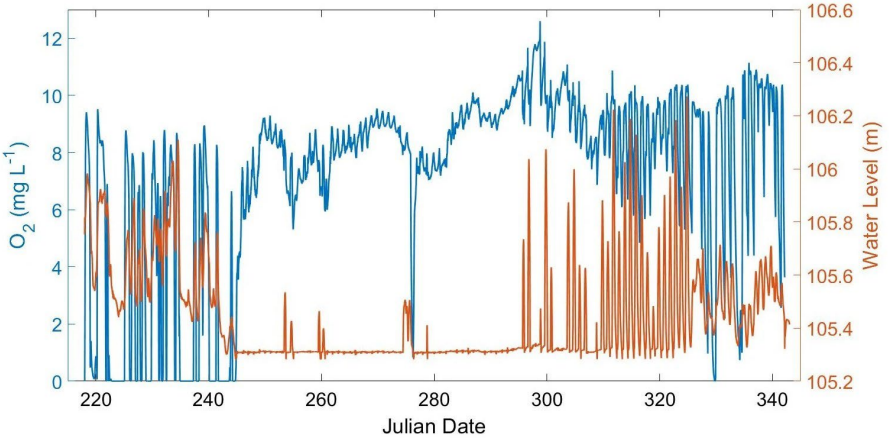

Figure 7. DO and water level recorded at ca. 20 cm depth by the in situ sensor. Periodic surface sediment water desaturation during an interval of relatively low river stage in September and October (Julian dates ~ 245-295; see Fig. 12) led to nearly continuous high measured DO concentrations, when at times the probe measured atmospheric rather than dissolved O_2 levels.

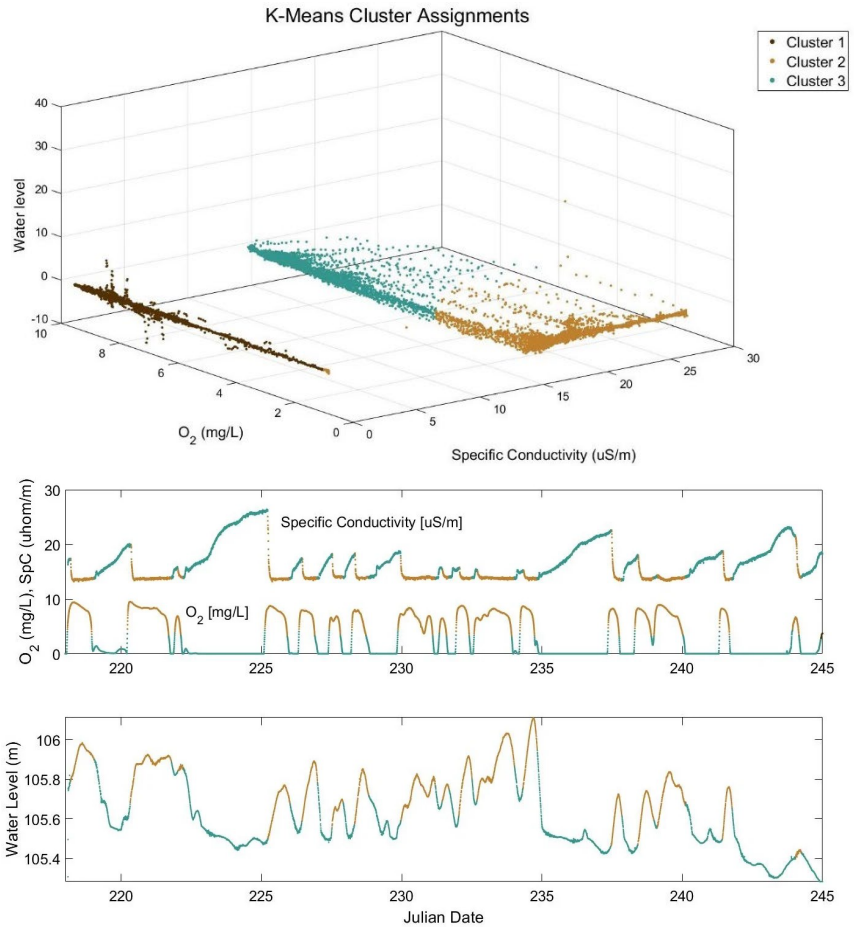

Figure 8. k-means clustering analysis of temporal change in situ DO, specific conductivity, and water level at ca. 20 cm depth in Hanford 300 Area sediments in Aug-Sep 2020.The colored lines in the lower panel indicate identified clusters.

REACTIVE TRANSPORT MODELING

POM Transport-Reaction Model

A one-dimensional advection-dispersion-reaction model was developed to simulate the transport and metabolism of POM (and DOM) within the upper 100 cm of the Hanford 300 Area riverbed. The central objective of the modeling wasto predict the potential impact of fresh POM influx on dissolved oxygen (DO) distributions. Key to this analysis was inclusion of periodic changes in the direction (either into or out of the sediment) and rate of fluid flow within the riverbed (see Hydrological Modeling section below). A summary of the operation of the POM transport-reaction model is provided in Appendix 1.

The model considers suspended (mobile) POM, sorbed/filtered (immobile) POM, dissolved organic matter (DOM) present in the river water, and DOM that originates from POM decay (Fig. 9). The representation of POM sorption and fitration is based on

the results of the POM transport experiments (Fig. 6), with parameter values adjusted to reproduced obsereved POM trap results (Fig. 5). Both POM and DOM degradation are treated as first-order reactions (Fig. 10), with rate constants determined from laboratory incubation experiments with Hanford 300 Area sediments amended with freshly-grown periphyton POM (Stern et al., 2021). The rate constants determined at room temperature (22C) were adjusted for in situ temperature assuming a Q10 value of 2.

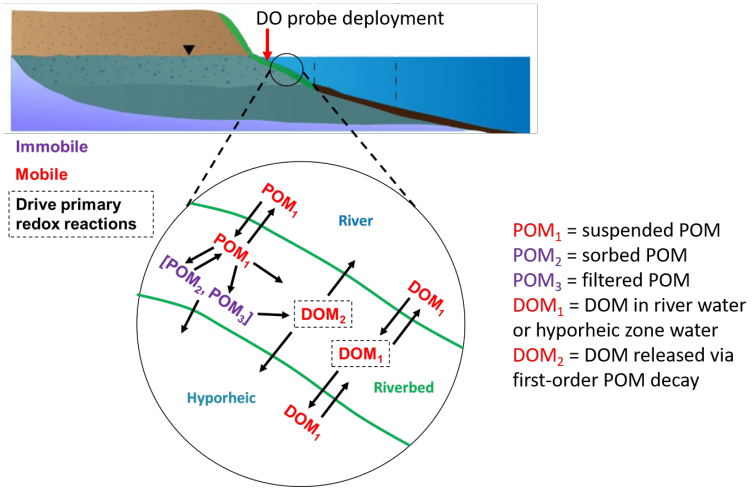

Fig. 9. Diagram illustrating the coupled POM-DOM degradation model.

Degradation of DOM drives a sequence of primary redox reactions (Fig. 11) according to the "Modified Monod" approach (Fig. 10; Boudreau and Westrich, 1984; Van Cappellen and Wang, 1996; Hunter et al., 1998). The model includes a comprehensive set of "secondary redox reactions" by which reduced compounds generated via anaerobic metabolic pathways are re-oxidized (dashed lines in Fig. 11) through second-order reactions (Fig. 10) with higher redox potential electron acceptors. Inclusion of such reactions is crucial for proper simulation of highly dynamic redox environments such as 300 Area riverbed sediments.

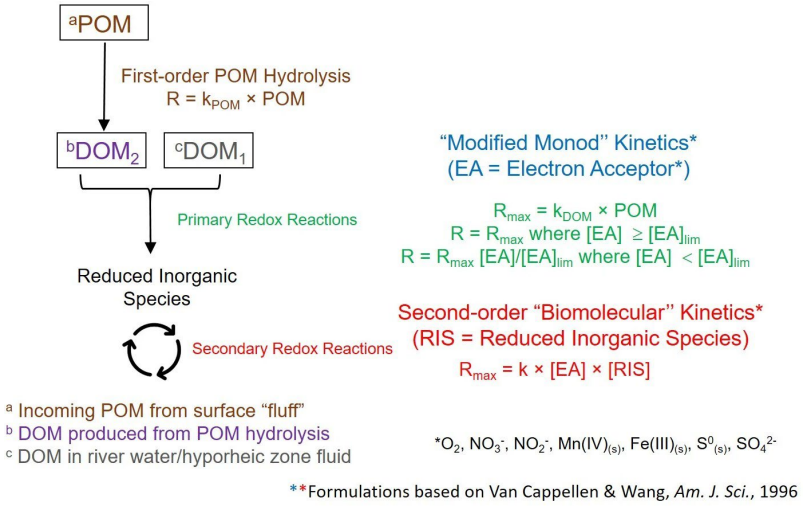

Figure 10. Reaction framework used to model POM degradation and associated redox cycling in Hanford 300 Area sediments.

Hydrological Modeling

The 1-D transport-reaction equations were solved via finite differences for a 100 cm spatial domain with 1 cm node spacing using the numerical method of lines (Boudreau, 1997). Fluid flow was driven by hourly river water level measurements at the 300 Area in 2020 (Fig. 12). The water level data was used to compute fluid flow rate and direction based on the relationship in Fig. 7 in Fritz and Arntzen (2007), which was determined through measurements of the hydraulic conductivity of the upper ca. 1 m of 300 Area sediments. The dashed line in

Fig. 12 illustrates the water level at which flow was assumed reverse direction (positive corresponds to flow into the riverbed). This approach represents an over-simplification due to hysteresis caused by the damped response of the aquifer water level relative to the river stage (Arntzen et al., 2006), and will in due course be replaced with a model of fluid flow based on both measured river stage and measured groundwater hydraulic head in the vicinity of the 300 Area (Zachara et al., 2020).

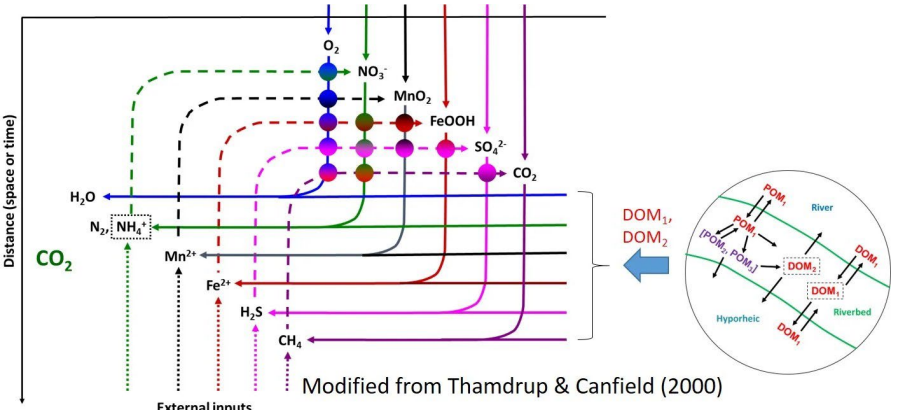

Figure 11. "Train station" diagram of the coupling of primary (solid lines) and secondary (dashed lines) redox reactions in sediments. Modified from Fig. 6.1 in Thamdrup and Canfield (2000).

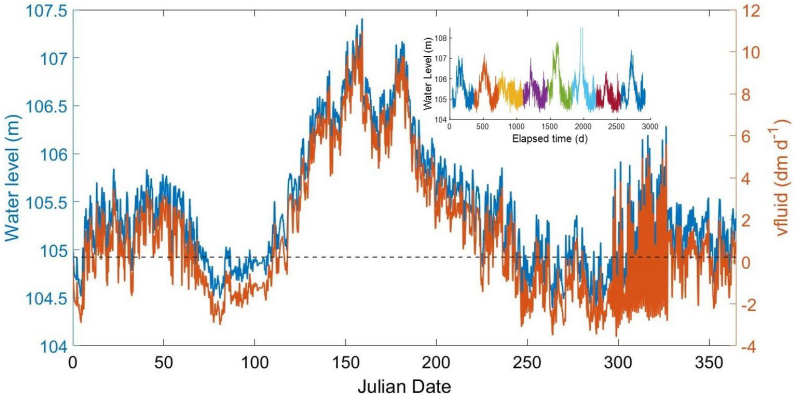

Figure 12. Measured (hourly) water level (data provided by H. Ren, PNNL SFA team) and estimated fluid flow rate/direction at the Hanford 300 Area site in 2020. The dashed line shows the water level at which flow direction was assumed to reverse, with postive rates going into the riverbed. Inset shows time series of water levels from 2013 through 2020.

Boundary conditions for solutes in the riverwater and groundwater/hyporheic zone fluid were established based on previous publications (Stegen et al., 2016) and the PNNL SFA database. POM input to the riverbed was simulated by assuming a fixed upper boundary supsended POC concentration of 1 mmol C/dm3 fluid. This boundary condition corresponds to the suspended "fluff" layer illustrated in Fig. 3. The suspended "fluff" concentration is consistent with measurements made on suspended materials collected in the vicinity of the riverbed in February 2020 (see photo in upper right corner of Fig. 4). Here again this is an over-simplification, as the abundance and organic content of material at or near the riverbed surface is likely to vary significantly over an annual cycle. However, runs of the transport-reaction model over time periods (30 or 40 d) corresponding to the two POM trap deployments produced results generally consistent with the POM trap results (Fig. 5).

MODELING RESULTS, INTERPRETATION, & CONCLUSIONS

Overview

The basic goal of the transport-reaction modeling was to evaluate whether or not POM input and degradation could play a role in producing anoxic conditions in the upper few dm of the riverbed (Fig. 7). The observation of sediment anoxia was unexpected given the high rates of fluid flow into and out of the riverbed (Fig. 12), and the fact that both the riverwater and the groundwater and deeper hyporheic zone fluid are rich in DO (Song et al., 2018; Kaufman et al., 2021).

Existing models of organic matter metabolism in Hanford 300 Area sediments assume either that metabolism is driven by (1) degradation of soluble DOM (e.g. Song et al., 2018), or (2) degradation of riverwater DOM together with a pool of POM that is renewed by input/burial of terrestrial organic matter (Yang et al., 2018). The latter assumption is problematic given that no major deposition or redistribution of alluvium sediments has take place since emplacement of the upstream hydroelectric power dams in the 1950s (Fecht et al., 2004). Thus, any relic pool of POM in the sediment must be highly depleted in POM. This creates a disconnect in that the Yang et al. (2018) analysis suggests that this relic POM turns over on a time scale of less than one year. These observations sets the stage for our investigation of the possible influence of mobile fresh POM input on sediment DO consumption.

Can DOM metabolism alone create anoxia?

A key first test for the model was to ask if, based on estimated fluid flux rates (Fig. 12) and known river/groundwater end-member DOC concentrations (ca. 0.1 and 0.01 mM, respectively; Stegen et al., 2016), DOM metabolism alone could produce anoxic conditions over an annual cycle. The results (Fig. 13) suggest that this is **NOT** the case. Sustained river water input was associated with periods of only partial DO depletion. On shorter time-scales (not evident in Fig. 13), transient slow-down in flow rate and eventual reversal of flow direction did lead to changes in DO concentration that are qualitatively analogous to DO measurements on fluids pumped from piezometers at the 300 Area site in 2018 (Kaufman et al., 2021). However, DO levels never fell to values lower than ca. 7.5 mg/L.

Influence of advective POM input

Simulations that included advective POM input and degradation produced periods of transient anoxia within the upper several dm of the riverbed (Fig. 14). Sorbed/filtered POM accumulated in the upper ca. 10 cm of sediment during

periods of sustained river water intrusion during the spring and early summer. Degradation of this material led to release of labile DOM that was transported throughout the sediment column. Metabolism of this material led to DO depletion that lagged the main peak in POM accumulation by ca. 1 month.

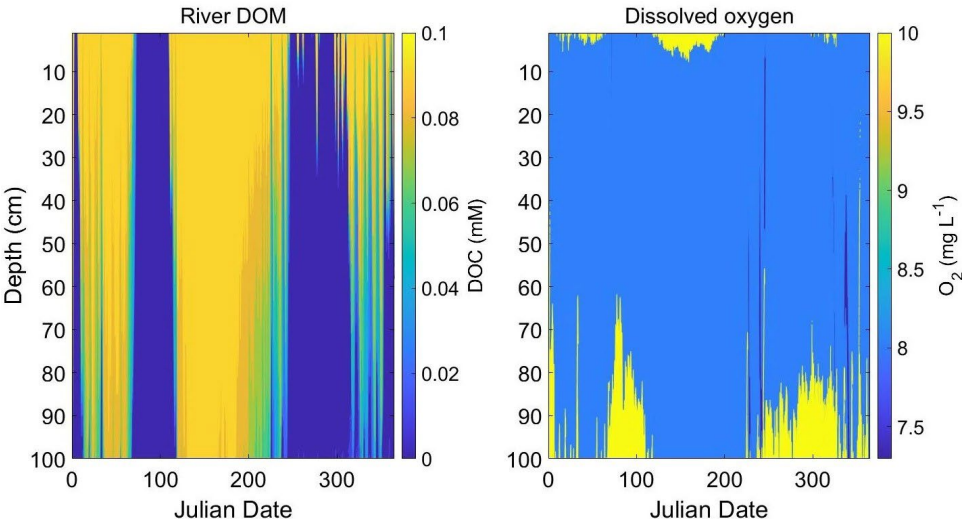

Figure 13. Measured (hourly) water level (data provided by H. Ren, PNNL SFA team) and estimated fluid flow rate/direction at the Hanford 300 Area site in 2020. The dashed line shows the water level at which flow direction was assumed to reverse, with postive rates going into the riverbed. Inset shows time series of water levels from 2013 through 2020.

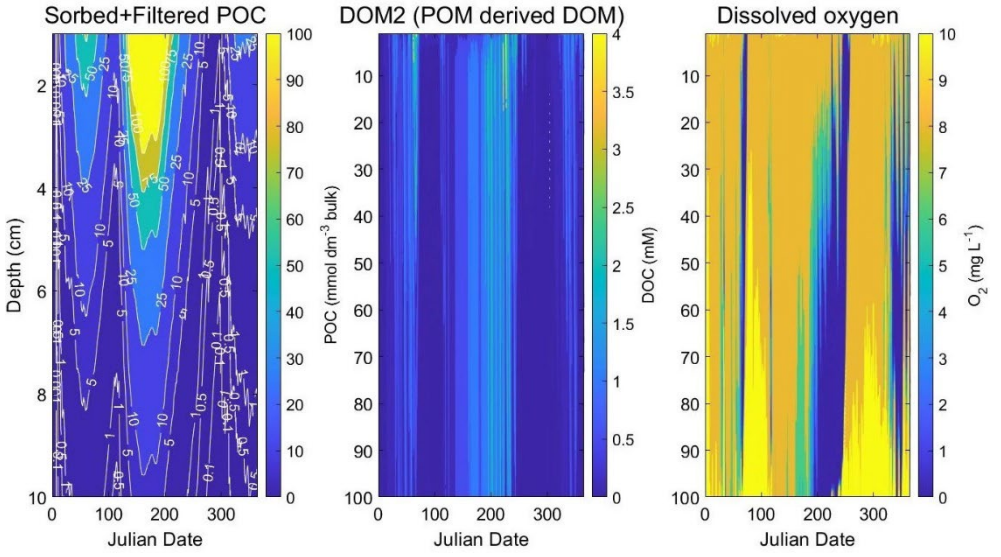

Figure 14. Simulated sorbed/filtered POM, POM-derived DOM (DOM2 in Fig. 9), and DO distrubtions over the 2020 water cycle.

On a shorter time scale (hours to days), changes in fluid flow rate and direction were associated with spikes in DO analogous to those observed during the Aug-Sep in situ DO probe deployments (Fig. 15). The model predicted co-variations in water level, specific conductivity, and DO qualitatively similar to those recorded during the in situ probe deployments. Declining rates of river water intrusion were associated with decreasing DO and increasing specific conductivity, reflecting the balance of forces between OM metabolism and DO resupply.

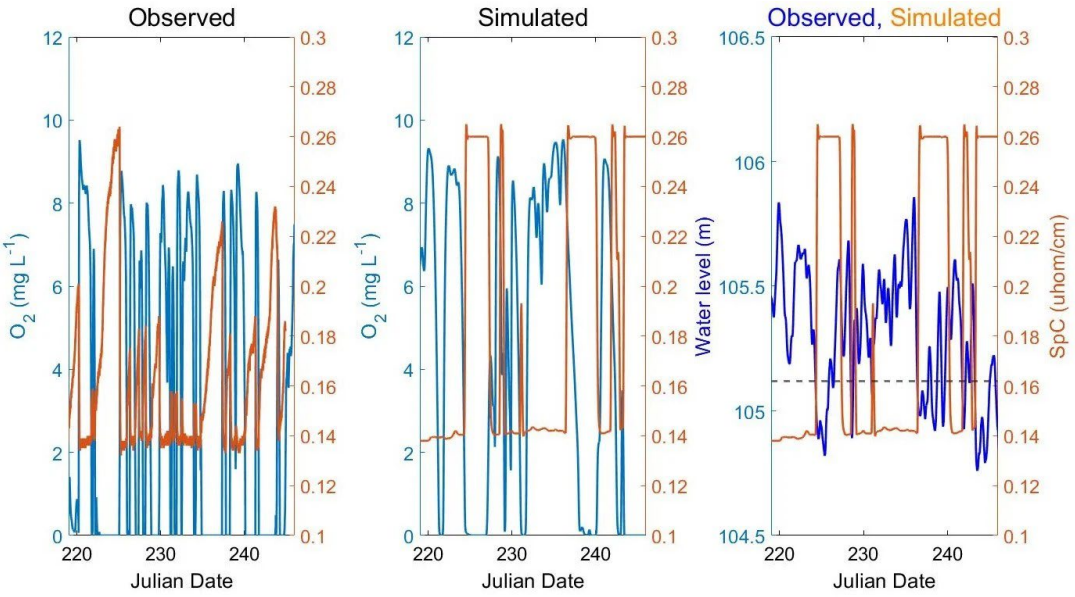

Figure 15. Observed and simulated DO and specific conductivity during the Aug-Sep 2020 in situ DO probe deployment. The water levels shown in the right-most panel are those used to drive fluid flow,

CONCLUSIONS

The results of our simulations indicate that DOM metabolism alone cannot account for the observation of periodic anoxic conditions within the upper few dm of Hanford 300 Ara riverbed sediments. In addition, the appeal to input/burial of terrestrial organic matter as a driver of sediment metabolism is inconsistent with the fact that no major depositional or redistrubtion of alluvium sediment has taken place for several decades in the HR of the CR. Thus, our concept of advective input of mobile suspended (colloidal) POM in the upper few dm of the riverbed, together with its degradation to mobile DOM that drives metabolism throughout the sediment column, provides a plausible explanation for the in situ DO sensor results. Collectively our results suggest a complex interplay between fluid flow rate/direction and DO distribution that has important implications for riverbed biogeochemical dynamics at a variety of spatial and temporal scales. The depletion of DO triggered the onset of anaerobic metabolic pathways and changes in N redox cycling specifically during time periods when rates of OM processing were maximal (data not shown). Whether or not

these changes occur in situ and are widespread in the HR and other analogous large river systems remains to be determined, e.g. through more sophisticated hydrobiogeochemical modeling together with in situ observation and experimentation.

Acknowledgments

This research was supported by the U.S. Department of Energy, Office of Biological and Environmental Research, Subsurface Biogeochemical Research (SBR) program through grants DE-SC0016217 and DE-SC0020309, (SBIR) program grant DE-SC0017129, and by the SBR Scientific Focus Area at PNNL. We are grateful to PNNL SFA personnel (James Stegen, Emily Graham, Tim Scheibe, Huiying Ren, Zhangshuan Hou, Douglas McFarland, Brandon Boehnke) for providing information and guidance on the development and interpretation of our experimental and modeling approaches and results.

REFERENCES

Arntzen, E. V., D. R. Geist, and P. E. Dresel. 2006. Effects of fluctuating river flow on groundwater/surface water mixing in the hyporheic zone of a regulated, large cobble bed river. River Res. and Applic. 22:937-946.

Boano, F., J. W. Harvey, A. Marion, A. I. Packman, R. Revelli, L. Ridolfi, and A. Worman. 2014. Hyporheic flow and transport processes: Mechanisms, models, and biogeochemical implications. Rev. Geophys. 52:603-679.

Boudreau, B. P. 1997. Diagenetic Models and Their Implementation. Springer, New York.

Boudreau, B. P., and J. T. Westrich. 1984. The dependence of bacterial sulfate reduction on sulfate concertation in marine sedimenmts. Geochim. Cosmochim. Acta 48:2503-2516.

Brunke, M. 1999. Colmation and depth filtration within streambeds: retention of particles in hyporheic interstices. Internat. Rev. Hydrobiol. 84:99-117.

Bulur, E. 2021. Particulate organic matter transport in experimental riverbed sediment columns. M.S. Thesis, Department of Geoscience, University of Wisconsin-Madison.

Bulur, E., E. E. Roden, S. A. Napieralski, S. P. Loheide, and M. Ginder-Vogel. 2021. Transport-reaction modeling of particulate organic matter dynamics in riverbed sediments. American Chemical Society Spring 2021 Meeting.

Fecht, K. R., T. E. Marceau, B. N. Bjornstad, D. G. Horton, and G. V. Last. 2004. Late Pleistocene- and Holocene-age Columbia River sediments and bedforms: Hanford Reach area. Washington: Bechtel Hanford, Incorporated.

Ghosh, R. N., R. Loloee, P. A. Askeland, and C. T. Weeks. 2019a. Optical sensor and sensing system for oxygen monitoring in fluids using molybdenum cluster phosphorescence. US Patent 10,520,435, issued Dec. 31, 2019.

Ghosh, R., T. Ball, M. J. Freeman, R. Loloee, C. McIntire, D. D. Shooltz, N. Ward, G. A. Gill, and A. Myers-Pigg. 2019b. Groundwater oxygen pulses within a coastal watershed: a potential driver of hot moments in the carbon cycle. American Geophysical Union Fall 2019 Meeting Abstract GC51H-0983.

Gooseff, M. N., R. Ghosh, R., E. M. Cantrell, M. J. Freeman, C. McIntire, and D. D. Shooltz,. 2019. How does streambed dissolved oxygen vary with hydrologic exchange: An evaluation from 15 months of high frequency measurements in the East River, CO. American Geophysical Union Fall 2019 Meeting Abstract B51M-2414.

Ghosh, R., T. Ball, M. J. Freeman, R. Loloee, C. McIntire, D. D. Shooltz, N. Ward, G. A. Gill, and A. Myers-Pigg. 2019b. How does streambed dissolved oxygen vary with hydrologic exchange: An evaluation from 15 months of high frequency measurements in the East River, CO. American Geophysical Union Fall 2019 Meeting Abstract B51M-2414.

Ghosh, R. N., P. A. Askeland, S. Kramer, and R. Loloee. 2011. Optical dissolved oxygen sensor utilizing molybdenum chloride cluster phosphorescence. Appl. Phys. Lett. 98.

Graham, E. B., A. R. Crump, D. W. Kennedy, E. Arntzen, S. Fansler, S. O. Purvine, C. D. Nicora, W. Nelson, M. M. Tfaily, and J. C. Stege. 2018. Multi 'omics comparison reveals metabolome biochemistry, not microbiome composition or gene expression, corresponds to elevated biogeochemical function in the hyporheic zone. Sci. Tot. Environ. 642:742-753.

Hanrahan, T. P., E. V. Arntzen, F. Khan, J. R. Stephenson, P. S. Titzler, and C. Tunnicliffe. 2007. Hyporheic exchange characteristics in Snake River aall Chinook salmon spawning areas. Report PNWD-3847. Battelle–Pacific Northwest Division Richland, Washington.

Harter, T., S. Wagner, and E. R. Atwill. 2000. Colloid transport and filtration of Cryptosporidium parvum in sandy soils and aquifer sediments. Environ. Sci. Technol. 34:62-70.

Hou, Z., W. C. Nelson, J. C. Stegen, C. J. Murray, E. Arntzen, A. R. Crump, D. W. Kennedy, M. C. Perkins, T. D. Scheibe, J. K. Fredrickson, and
J. M. Zachara. 2017. Geochemical and microbial community attributes in relation to hyporheic zone geological facies. Sci Rep 7.

Hunter, K. S., Y. Wang, and P. VanCappellen. 1998. Kinetic modeling of microbially-driven redox chemistry of subsurface environments: coupling transport, microbial metabolism and geochemistry. J. Hydrol. 209:53-80.

Kaufman, M. H., R. N. Ghosh, J. Grate, and J. Stegen. 2021. Dissolved oxygen dynamics reveal biogeochemical tipping points driven by river corridor hydrology. PLoS One. Submitted for publication.

Liu, Y. Y., F. Xu, and C. X. Liu. 2017. Coupled hydro-biogeochemical processes controlling Cr reductive immobilization in Columbia River hyporheic zone. Environ. Sci. Technol. 51:1508-1517.

Moser, D. P., J. K. Fredrickson, D. R. Geist, E. V. Arntzen, A. D. Peacock, S.-M. W. Li, T. Spadoni, and J. P. McKinley. 2003. Biogeochemical processes and microbial

characteristics across groundwater-surface water boundaries of the Hanford Reach of the Columbia River. Environ. Sci. Technol. 37:5127-5134.

Song, X. H., X. Y. Chen, J. Stegen, G. Hammond, H. S. Song, H. Dai, E. Graham, and J. M. Zachara. 2018. Drought conditions maximize the impact of high-frequency flow variations on thermal regimes and biogeochemical function in the hyporheic zone. Wat. Resourc. Res. 54:7361-7382.

Stegen, J. C., A. Konopka, J. P. McKinley, C. Murray, X. Lin, and M. D. Miller. 2016. Coupling among microbial communities, biogeochemistry, and mineralogy across biogeochemical facies. Sci Rep 6:30553.

Stern, N., J. C. Stegen, E. B. Graham, A. Goldman, M. Ginder-Vogel, and E. E. Roden. 2021. Influence of fresh particulate organic matter input on riverbed sediment microbial metabolism. Biogeochemistry Manuscript in preparation.

Stern, N., M. Ginder-Vogel, J. C. Stegen, E. Arntzen, D. W. Kennedy, B. R. Larget, and E. E. Roden. 2017. Colonization habitat controls biomass, composition, and metabolic activity of attached microbial communities in the Columbia River hyporheic corridor. Appl Environ Microb 83:e00260-00217.

Thamdrup, B., and D. E. Canfield. 2000. Benthic respiration in aquatic sediments. In O. E. Sala, R. B. Jackson, H. A. Mooney, and R. W. Howarth (eds.). Methods in Ecosystem Science, pp. 86-103. Springer, New York.

VanCappellen, P., and Y. Wang. 1996. Cycling of iron and manganese in surface sediments: a general theory for the coupled transport and reaction of carbon, oxygen, nitrogen, sulfur, iron, and manganese. Am. J. Sci. 296:197-243.

Yang, C., Y. K. Zhang, Y. Y. Liu, X. F. Yang, and C. X. Liu. 2018. Model-based analysis of the effects of dam-Induced river water and groundwater interactions on hydro-biogeochemical transformation of redox xensitive contaminants in a hyporheic zone. Wat. Res. Resourc. 54:5973-5985.

Zachara, J. M., X. Y. Chen, C. Murray, and G. Hammond. 2016. River stage influences on uranium transport in a hydrologically dynamic groundwater-surface water transition zone. Wat. Resourc. Res. 52:1568-1590.

Zachara, J. M., X. Y. Chen, X. H. Song, P. Shuai, C. Murray, and C. T. Resch. 2020. Kilometer-Scale Hydrologic Exchange Flows in a Gravel Bed River Corridor and Their Implications to Solute Migration. Wat. Res. Resourc. 56.

Appendix 1: Simulation of POM Transport and Metabolism in Hanford 300 Area Riverbed Sediments

A preliminary 1-dimensional advection-dispersion-reaction model has been developed to simulate the transport and microbial metabolism of POM in riverbed sediments in the vicinity of the Hanford 300 Area study site. The primary purpose of the model is to illustrate key aspects of POM transport and metabolism that are expected to occur in the column experiments. However, the developed framework will be transferrable to multiscale biogeochemical models for the Hanford Reach of the Columbia river that are being developed by the PNNL SFA team.

Model description. The preliminary simulations depict alternating fluid flow into and out of the riverbed, using published information on water flux rates between the river and groundwater in the 300 Area (Fritz and Arntzen, 2007). Based on these measurements water flux into the riverbed (5 dm^3 dm^{-2} d^{-1}) was assumed to be 2-fold higher than fluid flow in the opposite direction (2.5 5 dm^3 dm^{-2} d^{-1}). The model depicts advective/dispersive transport of POM using colloid filtration theory, which incorporates filtration and sorption as previously described for *Cryptosporidium parvum* oocysts in sandy soils and aquifer sediments (Harter et al., 2000). POM transport parameters were derived from the results of a recently completed SBR exploratory project employing simulated riverbed sand columns (Bessey et al., 2019). Although these parameters may differ from those to be determined for the column experiments proposed here, they provided an adequate starting point for the preliminary simulations.

Table A1 provides a list of the primary dependent variable in the model, along with river water and groundwater boundary conditions for aqueous constituents. The initial sediment geochemical conditions used in the model are based on the report of Liu et al. (2017) on chromium reductive immobilization in 300 Area riverbed sediment, together with water chemistry data from Stegen et al. (2016). The latter paper was also used to define river water (RW) and hyporheic zone (HZ) boundary conditions.

The organic matter components of the model operate as follows (see Fig. A1). Two different pools of dissolved organic matter (DOM) are present in the riverbed: (1) DOM that enters from either the river or hyporheic zone through advective fluid flux (DOM_1); and (2) DOM that is produced during hydrolytic breakdown of POM (DOM_2). Particulate organic matter (POM) is composed of three pools: (1) mobile suspended POM that enters into and is transported within the riverbed (POM_1); (2) immobile POM that accumulates via reversible sorption to riverbed solids (POM_2); and immobile POM that accumulates via irreversible filtration (POM_3). The latter pool of POM consists of material present in the riverbed at the start of the simulation, as well as POM that accumulates during the simulation. First-order decay of POM_1, POM_2, and POM_3 releases DOM_2, whose metabolism (along with DOM_1) drives the primary redox reactions (Fig. A1). The POM degradation model was parameterized based on PNNL SFA-funded experiments with POM-amended vs. unamended fine-grained 300 Area riverbed sediment slurries under oxic (air) vs. anoxic (N_2) headspace conditions (Stern et al., 2019). These experiments showed that rate constants for POM metabolism were ca. 2-fold higher under oxic conditions. The model thus employs two sets of rate constants active above or below an assumed O_2 threshold of 1 μM.

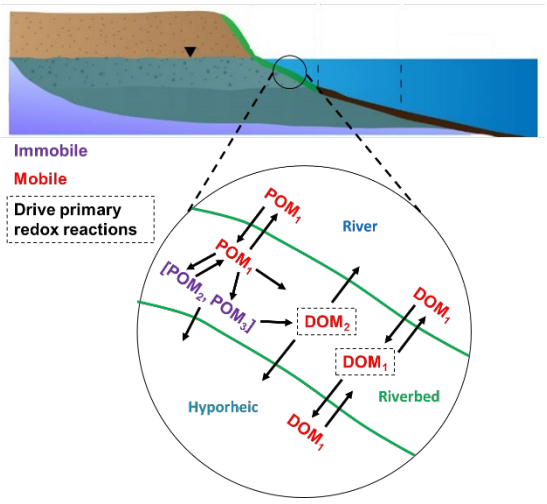

Fig. A1. Illustration of the operation of the organic matter components of the preliminary simulation model.

Table A1. Primary dependent variables in the riverbed POM transport and degradation model. Initial riverbed and river water/hyporheic zone boundary conditions (BC) are shown. Units are mol dm^{-3}_{aq} and mol dm^{-3}_{bulk} for mobile and immobile compounds, respectively.

Mobile	Fortran Name	Initial	River BC	Hyporheic BC	Source(s)
POM_1[a]	POM1	0.0	2.0×10^{-3}	0.0	Renteria et al., unpublished
DOM_1[b]	DOM1	1.0×10^{-4}	7.5×10^{-5}	1.0×10^{-4}	Stegen et al. (2016)
DOM_2[b]	DOM2	0.0	0.0	0.0	Arbitrary
O_2	O2	2.0×10^{-4}	2.0×10^{-4}	2.0×10^{-4}	PNNL SFA Team
NO_3^-	NO3	3.75×10^{-4}	3.75×10^{-5}	3.75×10^{-4}	Stegen et al. (2016)
NO_2^-	NO2	0.0	0.0	0.0	Arbitrary
SO_4^{2-}	SO4	2.0×10^{-4}	1.0×10^{-4}	2.0×10^{-4}	PNNL SFA Team
HCO_3^-	HCO3	1.0×10^{-3}	6.0×10^{-4}	3.0×10^{-4}	Stegen et al. (2016)
$Mn(II)_{aq}$	Mn2aq	0.0	0.0	0.0	Arbitrary
$Fe(II)_{aq}$	Fe2aq	0.0	0.0	0.0	Arbitrary
HS^-	HS	0.0	0.0	0.0	Arbitrary
CH_4	CH4	0.0	0.0	0.0	Arbitrary
NH_4^+	NH4	0.0	0.0	0.0	Arbitrary
Immobile					
POM_2[c]	POM2	0.0			Arbitrary
POM_3[d]	POM3	1.0×10^{-2}			Liu et al. (2017)
Mn(IV)[e]	Mn4	5.0×10^{-5}			Constrained
Fe(III)	Fe3	3.0×10^{-2}			Liu et al. (2017)
S^0	S0	0.0			Arbitrary
$Mn(II)_s$	Mn2s	0.0			Arbitrary
$Fe(II)_s$	Fe2s	0.0			Arbitrary
FeS	FeS	0.0			Arbitrary

[a] POM_1 = POM suspended in advecting fluid within the riverbed.
[b] DOM_1 = DOM entering the riverbed from the river or hyporheic zone; DOM_2 = DOM released during degradation of POM_1, POM_2.
[c] POM_2 = immobile POM that accumulates via reversible sorption to riverbed solids.
[d] POM_3 = immobile POM that accumulates immobile POM that accumulates via irreversible filtration.
[e] Assumed to be 60X less than $Fe(OH)_3$ (Canfield et al., 2005).

Degradation of DOM is coupled to utilization of oxygen, nitrate, manganese and iron oxides, elemental sulfur, and sulfate as electron acceptors for oxidation of organic carbon in a 50-cm column of riverbed sediment with a uniform porosity of 40 %. In the absence of external electron acceptors, organic carbon metabolism proceeds via methanogenesis. These reactions constitute the "primary redox reactions" in the model, which are driven by first-order decay of DOM. Competition among different primary redox reactions is depicted according to the "limiting concentration" (or Modified Monod) approach (VanCappellen and Wang, 1996; Wang and VanCappellen, 1996; Hunter et al., 1998), where utilization of a thermodynamically less favorable oxidant takes place only when the concentration of the more favorable oxidant falls below a defined limiting. Values for limiting concentrations for oxygen, nitrate, and sulfate were set equal to the values used in Hunter (1998) (20 μM, 5 μM, and 30 μM, respectively). The limiting concentration for Fe(III) oxide was determined based on the results of the above-mentioned POM addition experiment (Stern et al., 2019). The limiting concentrations for Mn(IV) and elemental S were arbitrarily set equal to those for Fe(III). Based on the results of Stern et al. (2019), and consistent with other studies with natural sediments (Roden, 2008) virtually all (95%) of the Fe(II) produced during Fe(III) reduction was

assumed to partition into the solid-phase. A similar assumption was made for partitioning of Mn(II) produced during Mn(IV) reduction.

The model incorporates the sediment nitrogen cycling framework developed by Akbarzadeh et al. (2018) for simulation of benthic N exchange in the Seine River (France). A combination of nitrate reduction coupled to N_2 formation (i.e. denitrification; 95% of total nitrate reduction) and dissimilatory nitrate reduction to ammonium (DNRA; 5% of total nitrate reduction) constitute the nitrate-associated primary redox reactions. Small amounts of nitrite (4% of total nitrate reduction) are assumed to "leak" into the system during denitrification and DNRA. Release of ammonium during OM decay (i.e. ammonification) occurs by assuming a C:N ratio of 10:1 for the labile DOM undergoing degradation. Nitrification takes place via a two-step process, whereby ammonium is first oxidized (by oxygen) to nitrite, and then nitrite is oxidized (again by oxygen) to nitrate. Finally, anaerobic ammonium oxidation (i.e. anammox) takes place via reaction of ammonium with nitrite produced via nitrate reduction and nitrification. Whereas Monod-style rate laws were employed by Akbarzadeh et al. (2018), our model employs the Modified Monod approach to depict nitrate reduction (see above) and second-order (bimolecular) rate laws for nitrification and anammox.

A variety of secondary redox reactions associated with reoxidation of reduced species were included in the model. Inclusion of such reactions (e.g. oxidation of Mn(II), Fe(II), HS^-, and FeS by O_2; oxidation of Fe(II) by Mn(IV); oxidation of HS^- by Mn(IV) and Fe(III) oxide) is crucial in models of sediment biogeochemical dynamics and redox zonation, because in many instances these reactions are likely to compete strongly with organic carbon oxidation for the consumption of electron acceptors (VanCappellen and Wang, 1996; Hunter et al., 1998). A realistic picture of the spatial/temporal zonation of microbially-driven redox reactions in sedimentary systems cannot be obtained if these reactions are ignored (Hunter et al., 1998). All of the secondary redox reactions described in Van Cappellen and Wang (1996) and Hunter (1998) were included in the model, plus others depicting (i) oxidation of Fe(II), HS^-, and FeS by NO_3^- and NO_2^-; (ii); conversion of solid-phase Fe(II) ($Fe(II)_s$) to FeS via reaction with HS^-; and (v) disproportionation of S^0 (to a mixture of SO_4^{2-} and HS^-) coupled to reaction of HS^- with Fe(III), Mn(IV) or $Fe(II)_s$. The secondary redox reactions were all depicted as second-order reactions. Rate constants for standard reactions were set equal to those used in Hunter (1998); rate constants for oxidation of dissolved and solid-phase Fe(II) by NO_3^- were derived from experimental studies in our laboratory (Weber et al., 2001); the rate constant for reaction of HS^- with $Fe(II)_s$ was assumed to be the same as that for the reaction of HS^- with Fe(III) oxide; and the rate constant for disproportionation of S^0 was derived from experimental studies of Thamdrup and colleagues (Bottcher and Thamdrup, 2001; Bottcher et al., 2001).

The coupled kinetic and advection/dispersion (mobile species) partial differential equations (PDEs) for the various dependent variables were solved by the numerical method of lines (Schiesser, 1991; Boudreau, 1997) using the stiff ODE integrator VODE (Brown et al., 1989). In this approach, the system of governing PDEs is discretized in space according to finite difference approximations (e.g. central differences), whereas the time step for integration is determined by the ODE solver so as to maintain a prescribed level of relative and absolute accuracy (in this case equal to 0.1 % and 10^{-12} mol dm^{-3}, respectively). The simulation was conducted using 100 node points across the 50-cm spatial domain. Constant concentration boundary conditions were assumed for mobile species at the top of the sediment column, and zero-gradient boundary conditions were assumed at the bottom of the spatial domain. The RW and HZ boundary conditions were used when the direction of fluid flow was into or out of the riverbed, respectively.

Simulation results. A series of sequential simulations were run to assess the impact of fresh POM input and transport on sediment metabolism, as well as the impact of flow reversals on biogeochemical conditions in the riverbed. After five days of input of RW with suspended POM, the flow direction was reversed and POM-free HZ fluid was introduced for a period of five days. This two-step sequence was then repeated for an overall simulation period of 20 days. The five-day interval was chosen based on the water flux results

reported by Fritz and Arntzen (2007) for the period of 3/1/05 to 3/23/05, where cyclic shifts between fluid transport into and out of the riverbed ranged from 3-6 days.

A key as yet constrained parameter in the model is the POM_1 boundary condition, i.e. the concentration of suspended POM at the riverbed surface. Although the bulk river water is typically relatively clear, as shown in Fig. 4 in the main text there are times when substantial amounts of fine-grained materials become resuspended. In addition, and more importantly, the photo in Fig. 4 reveals a cobble layer and surface sediment heavily colonized by periphyton, i.e. attached photosynthetic (and other microbial) biomass. One of the key field-scale goals of this project is to determine the abundance and accumulation rate of POM within the interstices of the cobble layer, i.e. material subject to advective transport into the permeable riverbed. For the purposes of the preliminary simulations, a modest suspended POM concentration of 24 mg C L^{-1} (2 mmol C L^{-1}) was assumed. This is a conservative value relative to the range of 50-70 mg C L^{-1} recently (April 2019) documented for the 300 Area surface "fluff" layer (Lupita et al., unpublished data; see further discussion below).

An initial simulation without POM_1 input (i.e. where only the 0.01 mol dm^{-3} of POM initially present in the sediment was metabolized) showed that all OM metabolism was mediated via aerobic respiration (data not shown). The subsequent simulations with POM input thus sought to assess how the input and transport of fresh POM would be expected to alter sediment OM metabolism and associated biogeochemical conditions. **The results suggest that input of POM during river water intrusion would indeed be expected to strongly influence riverbed biogeochemistry (Fig. A2A-C), leading to extensive accumulation of POM_3, depletion of oxygen and nitrate, and the onset of Mn(IV) and Fe(III) reduction within the upper 20 cm of sediment** (no sulfate/elemental S reduction or methanogenesis took place). Production of DOM_2 coupled to metabolism of the entrained POM led to accumulation of a few mM of DOC which underwent export to the HZ. In addition, as a result of the input and degradation of fresh POM, as well as the cessation of nitrification mid-way through the column, the concentration of ammonium in fluid being exported to the HZ (ca. 0.03 mmol dm^{-3}) was several-fold higher than in the absence of POM input. The predicted presence of mM levels of porewater DOC agrees with previous freeze core analyses (Moser et al., 2003). The predicted release of DOC is also consistent with our previous work with riverbed colonized sand packs (Stern et al., 2017), where DOC was released from POM that infiltrated into and was retained within

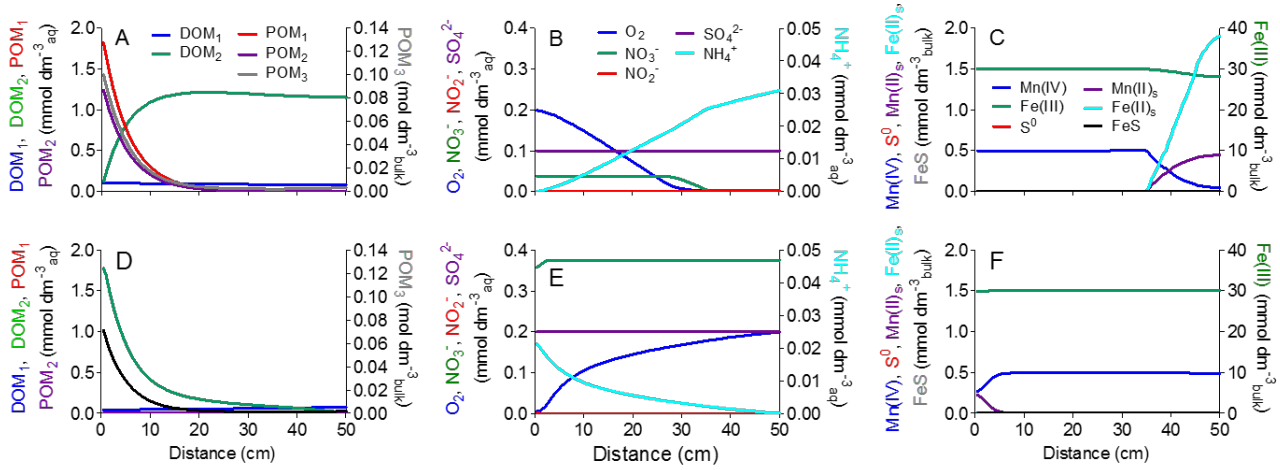

Fig. A2. Results from the preliminary riverbed POM transport and metabolism model. Panels A-C represent concentration profiles after the second cycle of POM input (days 10 to 15 of the simulation). Panels D-F represent concentration profiles after five days of flow reversal (i.e. input of POM-free HZ fluid) following the second cycle of POM input (days 15 to 20 of the simulation).

the sand packs (albeit at a much lower rate given that the sand packs were contained within a slotted metal tube and covered with light-shielding black mesh).

Reversal of the fluid flow direction (and input of POM-free HZ fluid) after POM input largely (but not completely) "reset" the biogeochemical conditions in the sediment column (Fig. 2D-F): input of oxygen and nitrate led to regeneration of Fe(III) and Mn(IV), and consumption of as well as export of DOM and ammonium to the river. These results suggest that redox oscillations are likely to be common in the near-surface riverbed, with important implications for carbon and nutrient cycling and hydrologic exchange within the hyporheic corridor.

In summary, we have produced a framework to simulate POM transport/metabolism and associated redox processes in a hypothetical riverbed sediment column that directly reflects the design of our planned column experiments (see below). The model can of course be used to simulate conditions in other types of columns, i.e. controls with no POM input, or ones with either no flow reversal or an inflow/outflow cycle different than five days. The overall framework will also be useful for extraction of rate constants for POM/DOM decay and other key reactions (e.g. nitrification) from the batch experiments (see below), as was done here using data from our previous POM addition experiments (Stern et al., 2019).

Table 2. Primary redox reactions included in the preliminary simulation model. OC corresponds to a single unit of organic carbon (i.e. CH_2O). The reactions apply to both aqueous (mobile) and solid-phase (immobile) OC. Reactions are written using the variable names in the Fortran 90 code.

Name	Reaction[a]	Fortran Name
Aerobic respiration	OC + O2 → HCO3	RO2C
Denitrification[b]	OC + 0.8NO3 → γ(HCO3 + 0.8(1 - α)N2) OC + 0.8NO3 → γ(HCO3 + 0.8αNO2)	RNO3N2C
Dissimilatory nitrate reduction to ammonium (DNRA)[b]	OC + 0.5NO3 → (1 - γ)(HCO3 + 0.5(1 - δ)NH4) OC + 0.5NO3 → (1 - γ)(HCO3 + 0.5δNH4)	RNO3N2C
Dissimilatory manganese reduction	OC + 2Mn4 → HCO3 + 2Mn2[c]	RMn4C
Dissimilatory iron reduction	OC + 4Fe3 → HCO3 + 4Fe2[c]	RFe3C
Dissimilatory elemental sulfur reduction	OC + 2S0 → HCO3 + 2HS	RSO4C
Dissimilatory elemental sulfur reduction	OC + 0.5SO4 → HCO3 + 0.5HS	RS0C
Methanogenesis	OC → 0.5HCO3 + 0.5CH4	RCH4C

[a] Only compounds that are included in the model are listed in the reactions; for example, compounds such as H^+, H_2O, not included in the model and therefore not listed in the reactions. Although N_2 is not included in the model, it is listed in denitrification reaction for clarity.

[b] γ = fraction of total nitrate reduction that proceeds through denitrification; α = fractional leakage of nitrite during denitrification; δ = fractional leakage of nitrite during DNRA (see Table 3).

[c] The model assumes that 95% of the Mn2 and Fe2 generated during OC oxidation is partitioned into the solid phase.

Table 3. Nitrogen cycling reactions included in the preliminary simulation model. OM represents a single unit of aqueous or solid-phase organic matter (i.e. CH_2ON_y), where y is ratio of ammonium release to organic carbon oxidation as dictated by an assumed C:N ratio of the organic matter. EA represents an arbitrary electron acceptor. The reactions apply to both aqueous (mobile) and solid-phase (immobile) OM. Reactions are written using the variable names in the Fortran 90 code.

Process	Reaction[a]	Fortran Name
Ammonification	OM + EA → yNH4	RNH4C
Nitrite leakage during denitrification	OM + 0.8NO3 → γ0.8αNO2	RNO2NO3N2C
Nitrite leakage during DNRA	OM + 0.8NO3 → (1 - γ)0.8δNO2	RNO2NO3NH4C
Nitrification step 1	NH4 + 1.5O2 → NO2	RNH4O2
Nitrification step 2	NO2 + 0.5O2 → NO3	RNO2O2
Anammox	NH4 + NO2 → N2	RNH4NO2

[a] See Table 2 for denitrification and DNRA reactions and explanation of parameters y, γ, α, and δ.

Table 4. Secondary redox reactions included in the preliminary simulation model. Note that each of these reactions is depicted by a second order (biomolecular) rate law.

Reaction	Fortran Name
Mn2aq + 0.5O2 → Mn4	RMn2aqO2
Mn2s + 0.5O2 → Mn4	RMn2sO2
Fe2aq + 0.25O2 → Fe3	RFe2aqO2
Fe2s + 0.25O2 → Fe3	RFe2sO2
HS + 2O2 → SO4	RHSO2
$S^0 + 1.5O_2 \rightarrow$ SO4	RS0O2
FeS + 2.25O2 → Fe3 + SO4	RFeSO2
CH4 + 2O2 → HCO3	RCH4O2
Fe2aq + 0.2NO3 → Fe3 + 0.1N2	RFe2aqNO3
Fe2s + 0.2NO3 → Fe3 + 0.1N2	RFe2sNO3
HS + 1.6NO3 → SO4 + 0.8N2	RHSNO3
S0 + 1.2NO3 → SO4 + 0.6N2	RS0NO3
FeS + 1.8NO3 → Fe3 + SO4 + 0.9N2	RFeSNO3
Fe2aq + 0.333NO2 → Fe3 + 0.167N2	RFe2aqNO2
Fe2s + 0.333NO2 → Fe3 + 0.167N2	RFe2sNO2
HS + 2.67NO2 → SO4 + 1.33N2	RHSNO2
S0 + 2NO2 → SO4 + N2	RS0NO2
FeS + 3NO2 → Fe3 + SO4 + 1.5N2	RFeSNO2
Fe2aq+ 0.5Mn4 → Fe3 + 0.5Mn2	RFe2aqMn4[a]
Fe2s+ 0.5Mn4 → Fe3 + 0.5Mn2	RFe2sMn4[a]
HS+ 4Mn4 → 4Mn2 + SO4	RHSMn4[a]
$FeS + 4.5MnO_2 \rightarrow 4.5Mn2 + SO4$	RFeSMn4[a]
HS + 2Fe3 → 2Fe2 + S0	RHSFe3[a]
$S^0 + 3Mn4 \rightarrow 3Mn2 + SO4$	RS0Mn4[a]
$3S^0 + 2Fe3 \rightarrow 2FeS + SO4$	RS0Fe3
$4S^0 + 3Fe2s \rightarrow SO4 + 3FeS$	RS0Fe2s
HS + Fe2s → FeS	RHSFe2s[b]

[a] The model assumes that 95% of the Mn2 and Fe2 generated during these reactions is partitioned into the solid phase.
[b] This is actually a mineral precipitation (FeS) reaction, which for the sake of simplicity is written as a biomolecular reaction between aqueous sulfide (HS) and solid-phase Fe(II) (Fe2s), where the latter is the overwhelmingly dominant form of Fe(II) such that the reaction between HS and aqueous Fe(II) (Fe2aq) can be ignored.

References

Akbarzadeh, Z., A. M. Laverman, F. Rezanezhad, M. Raimonet, E. Viollier, B. Shafei, and P. Van Cappellen. 2018. Benthic nitrite exchanges in the Seine River (France): An early diagenetic modeling analysis. Sci. Tot. Environ. 628-629:580-593.

Bessey, S., E. E. Roden, S. P. Loheide, and M. Ginder-Vogel. 2019. Transport of fresh particulate organic matter in simulated riverbed sediment columns. Manuscript in preparation.

Bottcher, M. E., and B. Thamdrup. 2001. Anaerobic sulfide oxidation and stable isotope fractionation associated with bacterial sulfur disproportionation in the presence of MnO_2. Geochim. Cosmochim. Acta 65:1573-1581.

Bottcher, M. E., B. Thamdrup, and T. W. Vennemann. 2001. Oxygen and sulfur isotope fractionation during anaerobic bacterial disproportionation of elemental sulfur. Geochim. Cosmochim. Acta 65:1601-1609.

Canfield, D. E., B. Thamdrup, and E. Kristensen. 2005. Aquatic Geomicrobiology. Elsevier, San Diego.

Fritz, B. G., and E. V. Arntzen. 2007. Effect of rapidly changing river stage on uranium flux through the hyporheic zone. Ground Water 45:753-760.

Harter, T., S. Wagner, and E. R. Atwill. 2000. Colloid transport and filtration of *Cryptosporidium parvum* in sandy soils and aquifer sediments. Environ. Sci. Technol. 34:62-70.

Hunter, K. S., Y. Wang, and P. VanCappellen. 1998. Kinetic modeling of microbially-driven redox chemistry of subsurface environments: coupling transport, microbial metabolism and geochemistry. J. Hydrol. 209:53-80.

Liu, Y. Y., F. Xu, and C. X. Liu. 2017. Coupled hydro-biogeochemical processes controlling Cr reductive immobilization in Columbia River hyporheic zone. Environ. Sci. Technol. 51:1508-1517.

Moser, D. P., J. K. Fredrickson, D. R. Geist, E. V. Arntzen, A. D. Peacock, S.-M. W. Li, T. Spadoni, and J. P. McKinley. 2003. Biogeochemical processes and microbial characteristics across groundwater-surface water boundaries of the Hanford Reach of the Columbia River. Environ. Sci. Technol. 37:5127-5134.

Roden, E. E. 2008. Microbiological controls on geochemical kinetics 1: Fundamentals and case study on microbial Fe(III) reduction. In S. L. Brantley, J. Kubicki, and A. F. White (eds.). Kinetics of Water-Rock Interactions, pp. 335-415. Springer, New York.

Stegen, J. C., J. K. Fredrickson, M. J. Wilkins, A. E. Konopka, W. C. Nelson, E. V. Arntzen, W. B. Chrisler, R. K. Chu, R. E. Danzak, S. J. Fansler, D. W. Kennedy, C. T. Resch, and M. Tfaily. 2016. Groundwater-surface water mixing shifts ecological assembly processes and stimulates organic carbon turnover. Nat. Comm. 7:Article 11237.

Stern, N., J. C. Stegen, E. B. Graham, A. Goldman, M. Ginder-Vogel, and E. E. Roden. 2019. Influence of fresh particulate organic matter input on riverbed sediment microbial metabolism. Manuscript in preparation.

Stern, N., M. Ginder-Vogel, J. C. Stegen, E. Arntzen, D. W. Kennedy, B. R. Larget, and E. E. Roden. 2017. Colonization habitat controls biomass, composition, and metabolic activity of attached microbial communities in the Columbia River hyporheic corridor. Appl Environ Microb 83:e00260-00217.

VanCappellen, P., and Y. Wang. 1996. Cycling of iron and manganese in surface sediments: a general theory for the coupled transport and reaction of carbon, oxygen, nitrogen, sulfur, iron, and manganese. Am. J. Sci. 296:197-243.

Wang, Y., and P. VanCappellen. 1996. A multicomponent reactive transport model of early diagenesis: Application to redox cycling in coastal marine sediments. Geochim. et Cosmochim Acta 60:2993-3014.